
Article:
Wang, Yafei, Liao, Yuanwei, Cabry, Christopher P. et al. (5 more authors) (2017) Highly efficient blueish-green fluorescent OLEDs based on AIE liquid crystal molecules:From ingenious molecular design to multifunction materials. Journal of Materials Chemistry C. pp. 3999-4008. ISSN 2050-7534

https://doi.org/10.1039/c7tc00034k

Highly Efficient Blueish-green Fluorescent OLEDs Based on AIE Liquid Crystal Molecules: From Ingenious Molecular Design to Multifunction Material

Yafei Wang[†‡], Yuanwei Liao[†], Christopher P. Cabry[#], Di Zhou[†], Guohua Xie[Δ*], Zuoming Qu[†], Duncan W Bruce[#*], Weiguo Zhu[‡*]*

[†]College of Chemistry, Key Lab of Environment-Friendly Chemistry and Application of the Ministry of Education, Xiangtan University, Xiangtan 411105, PR China

[‡]Jiangsu Key Laboratory of Environmentally Friendly Polymeric Materials, School of Materials Science & Engineering, Changzhou University, Changzhou 213164, PR China

[Δ]Hubei Collaborative Innovation Center for Advanced Organic Chemical Materials, Hubei Key Lab on Organic and Polymeric Optoelectronic Materials, Department of Chemistry, Wuhan University, Wuhan 430072, PR China

[#]Department of Chemistry, University of York, Heslington, York, YO10 5DD, UK

ABSTRACT: In order to seek the balance point between liquid crystalline and high efficiency emission, two novel aggregation-induced emission-based (AIE) liquid crystal materials of TPE-PBN and TPE-2PBN, which contains tetraphenylethene derivative as the emission core and 4-cynobiphenyl moiety as the mesogenic unit, were designed and prepared. Both simple molecules showed a mesophase at high temperature evidenced by polarised optical microscopy (POM), differential scanning calorimetry (DSC) and temperature-dependent X-ray diffraction (XRD). Simultaneously, TPE-PBN and TPE-2PBN presented clearly AIE characteristics in the blueish-green region and achieved the high emission quantum efficiency of 71% and 83% in solid state, respectively. Due to the self-assembly property of thermotropic liquid crystals, both compounds showed higher hole mobilities in the annealed films than in pristine films. Employing TPE-PBN and TPE-2PBN as the emitting materials, both non-doped devices and doped devices were fabricated. The TPE-PBN-based doped OLEDs showed a better device performance with an external quantum efficiency (EQE) of 4.1% which is among the highest EQE of the blue AIE fluorescent OLEDs.

KEYWORDS: Luminescent liquid crystal; Aggregation-induced emission; Tetraphenylethene; 4-Cyanobiphenyl; Organic light-emitting diodes

1 Introduction

Luminescent liquid crystal materials have gained much interest recently in both academic research and commercial endeavours owing to their characteristic self-organisation and emission properties.[1-3] These multi-functional materials can be employed as the emissive component in organic light-emitting diodes (OLEDs), in which the polarised electroluminescent emission (EL, polarised OLEDs) can be realised.[4-6] Furthermore, luminescent liquid crystal materials are available to enhance device performance due to the enhanced carrier mobilities caused by the long-range order consequent on liquid crystal self-organisation. Therefore, luminescent liquid crystal materials based OLEDs can be used as the backlight for liquid crystal displays (LCDs), with the prospect of replacing both the backlight and absorbing colour filters in conventional LCDs, which correspondingly reduces cost and enhances emission efficiency.[7,8] However, there are still some challenges for such materials relating to difficulties in molecular design, emission quenching in the solid state and few applications in the OLEDs field. Apparently then, there is much space to develop luminescent liquid crystal materials with highly-efficient emission.

To date, numerous efforts have been made to realise luminescent mesogens, with the most popular strategy being that of functionalising the emissive core with terminal flexible chains.[9-18] Kato and co-workers have developed many luminescent mesogens formed by a rigid, π-conjugated core (such as pyrene and anthracene) functionalised with peripheral alkoxy chains.[19-22] Although this strategy can effectively generate liquid crystallinity, the emission quantum yield (Φ_{PL}) is often rather low, probably due not only to non-radiative transitions *via* intramolecular vibration caused by the periphery flexible chains, but also the aggregation-induced quenching of the rigid π-conjugated core.

To enhance the emission efficiency of such materials, some transition metal ions, especially platinum, were introduced into liquid crystal materials.[23,24] Our previous works also put forth an effort to explore structure-property relationships of such Pt-based materials.[4,25-27] For example, some of us prepared the platinum-based metallomesogens that employed phenylpyridine derivatives as the cyclometallating ligand with acetylacetonato ancillary ligands.[28,29] However, platinum complexes are prone to aggregation because of their planar structure, which can lead to poor emission both in concentrated solution and in the neat film and/or to a heavily red-shifted emission from a MMLCT state.[30] Therefore, achieving luminescent mesogens with high emission efficiency (*e.g.* neat film and device) is a very important task.

Since Tang and co-workers first reported the phenomenon of aggregation-induced emission (AIE) where there is intense emission in the solid state rather than in dilute solution,[31,32] numerous emissive molecules with AIE characteristic have been prepared because of their potential application in OLEDs. Due to the twisted conformation of AIE molecules, the proposal to integrate AIE materials into liquid crystals has attracted increasing attention due to the highly efficient emission in the solid state. Recently, Tang and co-workers synthesised a tetraphenylethene (TPE)-based AIE liquid crystal molecule which was a green emitter in the solid state.[33] Unfortunately, OLEDs based on these AIE liquid crystal materials have not been reported and despite the remarkable progress in AIE-based luminescent mesogens, realising effective LC molecules with blue emission and high efficiency in OLEDs remains challenging.

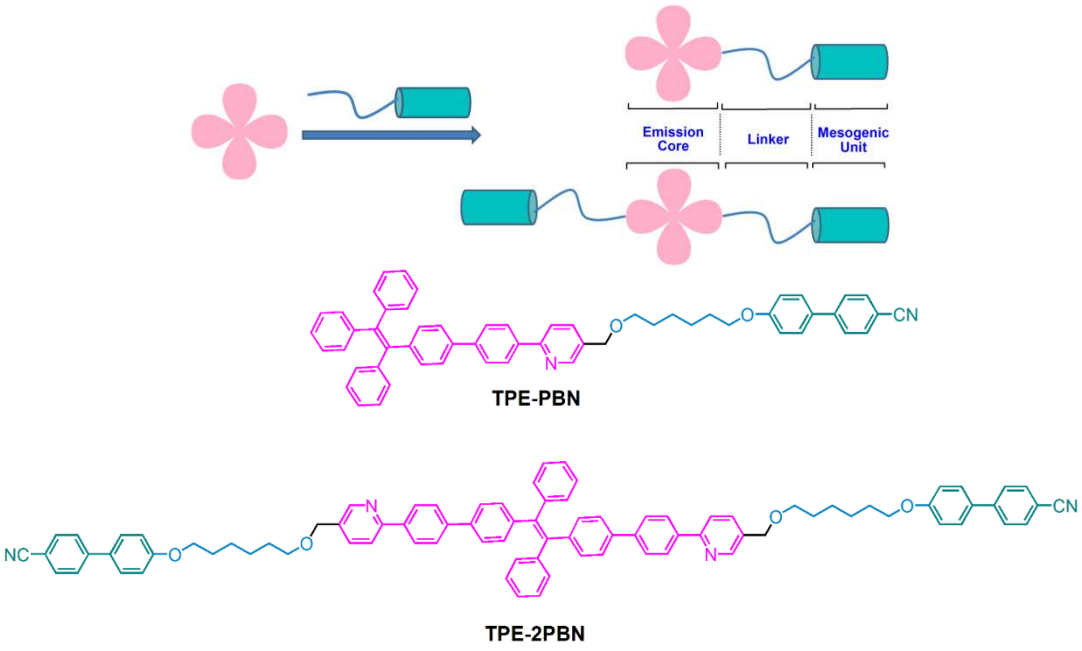

Chart 1. Modular design and molecule structures of luminescent AIE liquid-crystalline materials

In this contribution, we focus on AIE-based mesogens showing high-efficiency blueish green emission in OLEDs. As shown in Chart 1, the TPE unit is chosen owing it is typical of AIE luminogens and is readily synthesised. To enhance the emission efficiency, a phenylpyridine moiety conjugated with the TPE unit constitutes the emissive core due to the expanded π-conjugation. On the other hand, the 4-cyanobiphenyl unit is employed as the mesogenic unit, and then a flexible chain is used as the linking bridge between the emissive core and the mesogenic unit. Herein, two novel AIE-based luminescent mesogens of TPE-PBN and TPE-2PBN were designed and prepared, in which TPE represents tetraphenylethene-phenylpyridine derivative and PBN is the 4-cyanobiphenyl unit. Compared to emissive mesogens reported previously, a feature of these molecules is the presence of relatively few peripheral alkyl/alkoxy chains, which can reduce the intramolecular vibration. As expected, intense emissions with Φ_{PL} = 71% and 83% were recorded for TPE-PBN and TPE-2PBN, respectively, in the solid state. A mesophase was

observed for both molecules, evidenced by polarised optical microscopy, differential scanning calorimetry (DSC) and small-angle X-ray scattering (SAXS). Furthermore, the hole mobility of both compounds in annealed film, evaluated by space-charge limited current (SCLC) method, showed an order of magnitude higher than that of in pristine film. In order to explore the electroluminescent property of both compounds, non-doped and doped devices were fabricated based on TPE-PBN and TPE-2PBN. The TPE-PBN-based OLEDs showed blueish-green emission at 469 nm and achieved a better device performance with a maximum external quantum efficiency (*EQE*) of 4.1% which is among the highest *EQE* of the blue AIE fluorescent OLEDs.[34,35]

2 Experimental section

2.1 Materials and measurement

4'-Cyano-4-hydroxybiphenyl are commercial from Energy Chemical Company Ltd. Other reagents were purchased from J&K Chemical and Aladdin companies. All reactions were carried out under N_2 atmosphere. Compound 2 were prepared as described previously.[12] ^{1}H NMR and $^{13}C\{^1H\}$ NMR spectra were acquired using a Bruker Dex-400 NMR instrument using $CDCl_3$ as a solvent. Mass spectra (MS) were recorded on a Bruker Autoflex MALDI-TOF instrument using dithranol as a matrix. The UV-vis absorption and photoluminescence (PL) spectra were measured with a Varian Cray 50 and Perkin-Elmer LS50B luminescence spectrometer, respectively. The absolute fluorescence quantum yield was measured by using an absolute PL quantum yield spectrometer (Edinburg FLS-980 fluorescence spectrometer) with a calibrated integrating sphere and fluorescence lifetime measurements were recorded on the same spectrometer using time-correlated single photon counting (TCSPC). Thermogravimetric analysis (TGA) was carried out

with a NETZSCH STA449 from 25 °C to 600 °C at a heating rate of 20 °C min^{-1} under N_2 atmosphere. Differential scanning calorimetry (DSC) was measured at the phase transition temperature with a rate of 20 °C min^{-1} on the first heating circle and 10 °C min^{-1} on the first cooling and second heating process. Electrochemical response was evaluated by cyclic voltammetry with three typical electrodes in degassed CH_2Cl_2 solution with a rate of 100 mV s^{-1}. The CV system employed $Bu_4N[PF_6]$ as electrolyte; a platinum disk is used as the working electrode, platinum wire is regarded as the counter electrode and silver wire is used as the reference electrode. Ferrocenium/ferrocene (Fc^+/Fc) was used as the internal standard compound. Polarised optical microscopy was carried out using an Olympus BX50 Optical Microscope equipped with a Linkam Scientific LTS350 heating stage, Linkam LNP2 cooling pump and Linkam TMS92 controller. Small angle X-ray scattering was performed on a Bruker D8 Discover equipped with a Eurotherm temperature controlled, bored graphite rod furnace, custom built and integrated at the University of York.

2.2 Hole mobilities

The hole mobility was measured using the SCLC model with a devices configuration of ITO/PEDOT:PSS/Active Layer (100 nm)/MoO_3 (10 nm)/Ag (100 nm). The active layer is annealed for 30 mins at 165 ºC. The PEDOT:PSS was spin-coated onto the ITO glass at 4000 rpm. The active layer was spin-cast from dichlorobenzene (10 mg mL^{-1}) at 1000 rpm. A MoO_3 and Al cathode was then thermally evaporated under vacuum ($\sim 10^{-7}$ torr) through a shadow mask defining an active device area of ~0.03 cm^2. The SCLC is described by: $J = (9/8)\varepsilon_0\varepsilon_r\mu(V^2/d^3)$, where J is the current density, d is the film thickness of the active layer, μ_0 is the hole mobility, ε_r is the relative dielectric constant of the transport medium, ε_0 is the permittivity of free space (8.85×10^{-12} F m^{-1}), V is the internal voltage in the device.

2.3 Devices fabrication and characterisation

All the devices employing TPE-PBN and TPE-2PBN as the dopants were fabricated by a solution-processed approach. In these OLEDs, a layer of 30 nm-thick poly(3,4-ethylenedioxythiophene) polystyrene sulfonate (PEDOT:PSS) was spin-coated onto the pre-cleaned and patterned ITO substrate, which was utilised as hole-injecting layer. 1,3-Bis(*N*-carbazoly)benzene (mCP) was used as the host matrix, while 1,3,5-tri[(3-pyridyl)-phen-3-yl]benzene (TmPyPB) (40 nm layer) served as the electron-transporting layer. Liq and Al were used as the composite cathode. The electroluminescent (EL) spectra were recorded using a spectrascan spectroradiometer, Photo Research PR735. The features of the current density and brightness versus applied voltage were simultaneously obtained by combining a Keithley 2400 and PR735. The *EQE* was calculated from the luminance, current density, and EL spectrum, assuming a Lambertian distribution. The device configurations are as follows: ITO/PEDOT:PSS (40 nm)/the emitter layer/TmPyPB (50 nm)/Liq (1 nm)/Al (100 nm).

2.4 Synthesis

Synthesis of 1

A mixture of 4'-cyano-4-hydroxybiphenyl (4.99 g, 25.6 mmol), 1,6-dibromohexane (31.0 g, 128 mmol), K_2CO_3 (17.7 g, 128 mmol) and KI (127 mg, 0.77 mmol) were dissolved in acetone (200 mL) and heated under reflux for 24 h under N_2. After cooling to room temperature, the mixture was poured into water and extracted with CH_2Cl_2 (3×20 mL). The organic layer was collected and washed with water (3×20 mL), dried with anhydrous Na_2SO_4. The solvent was removed under vacuum, and then the residue was purified by column chromatography with petroleum ether (PE) as an eluent to get the compound 1 (colourless solid, 8.2 g, yield: 86%). ^{1}H NMR (400 MHz, $CDCl_3$), δ: 7.69 (d, J = 8.0 Hz, 2H), 7.64 (d, J = 8.0 Hz, 2H), 7.53 (d, J = 8.0

Hz, 2H), 6.99 (d, *J* = 8.6 Hz, 2H), 4.02 (t, *J* = 8.0 Hz, 2H), 3.44 (t, *J* = 8.0 Hz, 2H), 1.91 (t, *J* = 8.0 Hz, 2H), 1.83 (t, *J* = 8.0 Hz, 2H), 1.53 (t, *J* = 4 Hz, 4H). $^{13}C\{^{1}H\}$ NMR (100 MHz, CDCl3), δ (ppm): 159.71, 145.25, 132.59, 131.35, 128.37, 127.10, 119.15, 115.08, 110.05, 67.90, 33.86, 32.68, 29.06, 27.93, 25.31. MALDI-MS (m/z): calcd. 357.07; found.357.02.

Synthesis of 3

An addition of NaH (0.46 g, 19.0 mmol) to a solution of compound 2 (1.00 g, 3.80 mmol) in DMF (50 mL) at RT was stirred for 15 min. Compound 1 (1.55 g, 4.50 mmol) was added at 0 °C for 30 min, and then the mixture was allowed to warm to room temperature and was stirred for 24 h. The mixture was poured into water and extracted with CH_2Cl_2 (3×20 mL). The organic phase was washed with water for three times and dried with anhydrous Na_2SO_4. The solvent was removed *via* rotary evaporation under vacuum, and the residue was purified by column chromatography with PE/CH_2Cl_2 (2:1) as an eluent to get the compounds 3 (pale yellow powder, 2.06 g, yield: 84%).^{1}H NMR (400 MHz, $CDCl_3$), δ: 8.66 (s, 1H), 7.89 (d, *J* = 12.0 Hz, 2H), 7.78 (d, *J* = 8.0 Hz, 1H), 7.72 (d, *J* = 4.0 Hz, 1H), 7.70 (d, *J* = 4.0 Hz, 2H), 7.65 (d, *J* = 8.0 Hz, 2H), 7.61 (d, *J* = 8.0 Hz, 2H), 7.54 (d, *J* = 8.0 Hz, 2H), 7.00 (d, *J* = 8.0 Hz, 2H), 4.58 (s, 2H), 4.03 (t, *J* = 8.0 Hz, 2H), 3.56 (t, *J* = 8.0 Hz, 2H), 1.85 (t, *J* = 8.0 Hz, 2H), 1.71 (t, *J* = 8.0 Hz, 2H), 1.52 (t, *J* = 4.0 Hz, 4H). $^{13}C\{^{1}H\}$ NMR (100 MHz, CDCl3), δ (ppm): 159.75, 155.60, 149.14, 145.24, 138.04, 136.38, 132.82, 132.58, 131.90, 131.29, 128.43, 128.33, 127.07, 123.43, 120.00, 119.15, 115.08, 110.04, 70.66, 70.19, 68.01, 29.66, 29.17, 25.99, 25.91. MALDI-MS (m/z): calcd. 540.14; found.541.12.

General procedure for synthesis compound 5 and 7

A mixture of TPE with bromine substituent (compounds 4 and 6), bis(pinacolato)diboron, CH_3COOK and dichloro{1,1'-bis(diphenylphosphino)ferrocene}palladium(II) were dissolved in

1,4-dioxane was refluxed for 24 h. After cooling to room temperature, the mixture was poured into water and extracted with CH_2Cl_2 (3×20 mL). The organic phase was collected and washed with water (3×20 mL), dried with anhydrous Na_2SO_4. The solvent was removed under vacuum, and then the residue was purified by column chromatography.

5: PE/CH_2Cl_2 (5:1), colourless solid, 2.10 g, yield: 76%. ^{1}H NMR (400 MHz, $CDCl_3$), δ: 7.54 (d, *J* = 8.0 Hz, 2H), 7.09 (m, 10H), 7.01-7.04 (m, 7H), 1.32 (s, 12H). MALDI-MS (m/z): calcd. 458.24; found.457.70.

7: PE/CH_2Cl_2 (5:1), colourless solid, 720 mg, yield: 60%. ^{1}H NMR (400 MHz, $CDCl_3$), δ: 7.56 (d, *J* = 8.0 Hz, 4H), 7.10 (m, 6H), 7.04 (m, 8H), 1.31 (s, 24H). ^{13}C{^{1}H} NMR (100 MHz, CDCl3), δ (ppm): 146.74, 146.56, 143.52, 143.37, 141.24, 134.16, 134.07, 131.34, 130.70, 127.73, 127.63, 126.56, 126.49, 83.71, 83.52, 25.03, 24.89. MALDI-MS (m/z): calcd. 584.33; found.584.85.

General procedure for synthesis TPE-PBN and TPE-2PBN

To a dry round-bottom flask was added compound **5** (or **7**), compound 3 (1 mol. eq or 2 mol. eq, respectively), potassium carbonate solution (2 M), tetrakis(triphenylphosphine)palladium (0.03 eq or 0.06 mol. eq) and THF. The mixture was refluxed for 24 h or 2 days under nitrogen. After cooling to room temperature, the mixture was poured into water and extracted with CH_2Cl_2 (3×20 mL). The organic phase was washed with water for three times and dried with anhydrous Na_2SO_4. The solvent was removed via rotary evaporator under vacuum, and then the residue was purified by column chromatography.

TPE-PBN: PE/CH_2Cl_2 = 1:2, colourless solid, 197 mg, yield: 67%. ^{1}H NMR (400 MHz, $CDCl_3$), δ: 8.65 (s, 1H), 8.02 (d, *J* = 8.0 Hz, 2H), 7.76 (d, *J* = 8.0 Hz, 2H), 7.69-7.61 (m, 6H), 7.51 (d, *J* = 4.0 Hz, 2H), 7.41 (d, *J* = 8.0 Hz, 2H), 7.14-7.03 (m, 17H), 6.98 (d, *J* = 8.0 Hz, 2H), 4.56 (s, 2H),

4.01 (d, *J* = 8.0 Hz, 2H), 3.54 (t, *J* = 8.0 Hz, 2H), 1.83 (t, *J* = 8.0 Hz, 2H), 1.69 (t, *J* = 8.0 Hz, 2H), 1.50 (t, *J* = 4.0 Hz, 4H). $^{13}C\{^{1}H\}$ NMR (100 MHz, $CDCl_3$), δ(ppm): 159.78, 156.42, 149.13, 145.28, 143.77, 143.72, 143.14, 141.27, 141.17, 140.49, 138.14, 137.86, 136.32, 132.58, 132.38, 131.88, 131.44, 131.37, 131.30, 128.34, 127.82, 127.74, 127.67, 127.18, 127.17, 127.08, 126.56, 126.47, 126.16, 120.12, 119.13, 115.11, 110.05, 70.59, 70.29, 68.03, 29.74, 29.68, 29.18, 26.00, 25.91. MALDI-MS (m/z): calcd. 792.37 found. 793.37.

TPE-2PBN: $CHCl_3$/THF = 100:1, light yellow solid, 250 mg, yield: 60%. ^{1}H NMR (400 MHz, $CDCl_3$), δ: 8.68 (s, 2H), 8.06 (d, *J* = 8.0 Hz, 4H), 7.78 (d, *J* = 4.0 Hz, 4H), 7.72-7.66 (m, 12H), 7.54 (d, *J* = 8.0 Hz, 4H), 7.45 (d, *J* = 8.0 Hz, 4H), 7.18-7.14 (m, 14H), 7.01 (d, *J* = 12.0 Hz, 4H), 4.59 (s, 4H), 4.03 (d, *J* = 8.0 Hz, 4H), 3.56 (d, *J* = 8.0 Hz, 4H), 1.85 (t, *J* = 8.0 Hz, 4H), 1.71 (t, *J* = 8.0 Hz, 4H), 1.52 (t, *J* = 4.0 Hz, 8H). $^{13}C\{^{1}H\}$ NMR (100 MHz, $CDCl_3$), δ(ppm): 159.78, 156.42, 149.13, 145.28, 143.77, 143.72, 143.14, 141.27, 141.17, 140.49, 138.14, 137.86, 136.32, 132.58, 132.38, 131.88, 131.44, 131.37, 131.30, 128.34, 127.82, 127.74, 127.67, 127.18, 127.17, 127.08, 126.56, 126.47, 126.16, 120.12, 119.13, 115.11, 110.05, 70.59, 70.29, 68.03, 29.74, 29.68, 29.18, 26.00, 25.91.MALDI-MS (m/z): calcd. 1252.59; found.1252.35.

3 Results and discussion

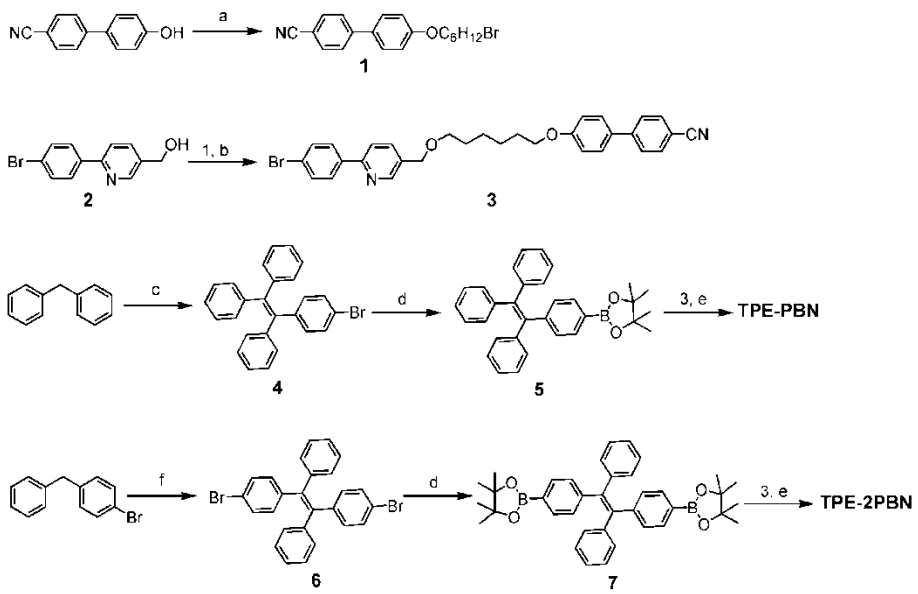

Reaction conditions: (a) 1,6-dibromohexane, K_2CO_3, KI, acetone, 65 ^oC, 24 h, yield, 86%; (b) (6-(4-bromophenyl)pyridin-3-yl) methanol, NaH, DMF, 0 ^oC, 30 min, yield: 84%; (c) i) (4-bromophenyl)(phenyl)methanone, *n*-butyllithium, THF, 0 ^oC, 30 min; ii) *p*-toluenesulfonic acid, toluene, 110 ^oC, 3-4 h, yield: 66%; (d) bis(pinacolato)diboron, CH_3COOK, [$PdCl_2$(dppf)], 1,4-dioxane, 80 ^oC, 24 h, yield: 5: 76%, 7: 60%; (e) [$Pd(PPh_3)_4$], 2 M K_2CO_3, THF, 65 ^oC, 24 h, yield, TPE-PBN: 67%, TPE-2PBN: 60%; (f) Zn, $TiCl_4$, THF, –78 ^oC, 30 min, yield: 83%.

Scheme 1. Synthetic route for both PBN-TPE and PBN-TPE-PBN

3.1 Synthesis

The synthetic routes for TPE-PBN and TPE-2PBN are depicted in Scheme 1, and the detailed procedures are presented in Supporting Information (ESI†). Started from the commercial 4'-cyano-4-hydroxybiphenyl, compound **1** was prepared by the Williamson etherification with K_2CO_3 in solution in acetone. Then compound **1** was reacted with compound **2**[36] to give precursor **3** in 84% yield. TPE with bromine substituents were synthesised according to previous reports.[37] In the presence of [$PdCl_2$(dppf)], the Miyaura borylation reaction between bromo-substituted TPE derivatives and bis(pinacolato)diboron yielded borinic esters (5 and 7) which reacted with precursor **3** afforded the target compounds *via* typical Suzuki coupling reactions in 60-67%

yields. All target compounds were characterised by ^{1}H and $^{13}C\{^{1}H\}$ NMR spectroscopy and TOF-MS, as shown in Supporting Information (ESI†).

3.2 Thermal behaviour

Both compounds exhibit good thermal stability and show a 5% weight loss at temperatures above 330 ºC (Table 1). The phase transition behaviour of both compounds was evaluated by optical microscopy and DSC and the phases were further studied using small-angle X-ray scattering (SAXS); thermal data are listed in Table 1.

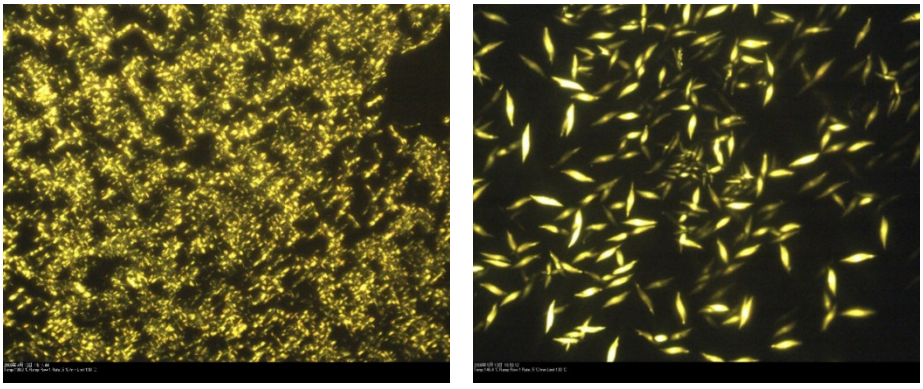

Figure 1. POM images of TPE-PBN (left, 138 ^{o}C) and TPE-2PBN (right, 148 ^{o}C) recorded on cooling process

Table 1 Phase-transition temperatures of TPE-PBN and TPE-2PBN

Compound	Phase sequence	T_{onset}/^{0}C	T_{d}/^{0}C
TPE-PBN	Cr-Cr'	54	362
	Cr'-Sm	156	
	Sm-Iso	185	
TPE-2PBN	Cr-oblique	146	335
	oblique-Iso	174	

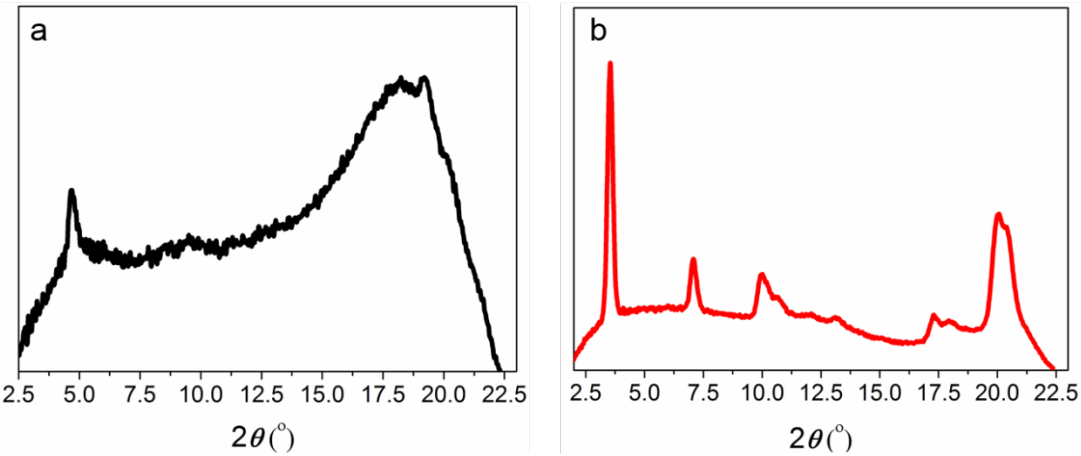

Figure 2. Temperature-dependent XRD for TPE-PBN (a, 140 °C) and TPE-2PBN (b, 170 °C) upon heating processes

On heating TPE-BPN, melts at 156 °C to give a birefringent fluid that clears at 185 °C. The SAXS pattern is not very helpful (see Figure 2a) but does contain a single, small-angle reflection at $2\theta = 4.5°$, which corresponds to a *d*-spacing of 19.6 Å, which is close to half of the estimated molecular length, suggesting a heavily interdigitated arrangement, which is quite common with mesogens containing a cyanobiphenyl moiety. Note that there is a weak feature at $2\theta \approx 9.5°$, which would correspond to a distance of *ca* 9.3 Å. This is close to twice the smaller angle reflection and has a similar peak width; as such it is tentatively identified as a *d*(002) reflection. In the absence of a good texture (precluded by the relatively high viscosity) it is difficult to say anything further about the nature of the phase except to suggest that it is lamellar in nature.

Turning now to TPE-2BPN, this compound softens from around 60 °C, but it is only at 140 °C that it melts and becomes more fluid, clearing at 174 °C. The texture (Figure 1, right) is rather featureless but the sample can be sheared, which affects the apparent alignment. The SAXS data (Figure 2b) show a strong, sharp reflection at $2\theta = 3.54°$ and then several mid-angle reflections as well as structured reflections around $2\theta \approx 20°$, which suggest that while this is clearly a mesophase, it is less apparent that it is a true LC phase. Using the LCDiXRay application from

Godbert *et al*.,[38] it is possible to index the reflection in both a rectangular and an oblique lattice (data in ESI†). The data fit better with the oblique lattice and so this is the assignment made. It is often the case that oblique lattices are associated with columnar phases, but in this case, the nature of the compounds would not be consistent with formation of a columnar arrangement. However, in our view the idea of what is a columnar phase is applied perhaps too liberally and so in the case, the phase would be assigned as a ribbon phase with an oblique 2D arrangement. This is entirely consistent with the analogy between Col_r, SmÃ and B_1 phases, all of which are rectangular and essentially have very similar if not the same arrangement.

3.3 Photophysical property

The absorption spectra of both compounds measured in THF at room temperature are shown in Figure S4 (ESI†), and the relevant data are listed in Table 2. Intense absorption bands between 250 and 400 nm are observed for both compounds, which are attributed to the π-π electron transition of aromatic rings in the TPE core.[39] A very weak absorption band in the range of 400-525 nm is detected for TPE-PBN, probably it is assigned to the intramolecular charge transfer (ICT) process caused by the separated HOMO (highest occupied molecular orbitals) and LUMO (lowest unoccupied molecular orbitals) (*vide infra*). Compared with the TPE-PBN, TPE-2PBN exhibits a blue-shifted absorption edge, probably due to the increased twist structure from TPE-PBN to TPE-2PBN, evidenced by density functional theory calculation (DFT, *vide infra*).

Table 2 photophysical data of TPE-PBN and TPE-2PBN

Compound	**Absorption[a] /nm**	**Emission[b] /nm**	**Lifetime[c] /ns**	Φ_{PL}[d] **%**	E_{ox}[e] **/V**	E_{red}[e] **/V**
TPE-PBN	300, 339,	479	1.51	71	1.30	-1.84

	441, 501					
TPE-2PBN	300, 345	490	1.44	83	1.22	-1.72

a: measured in THF solution; b: in neat film; c: in toluene solution; d: in solid state; e: in CH_2Cl_2 solution, the data collected from the maximum peak *verse* Fc/Fc^+;

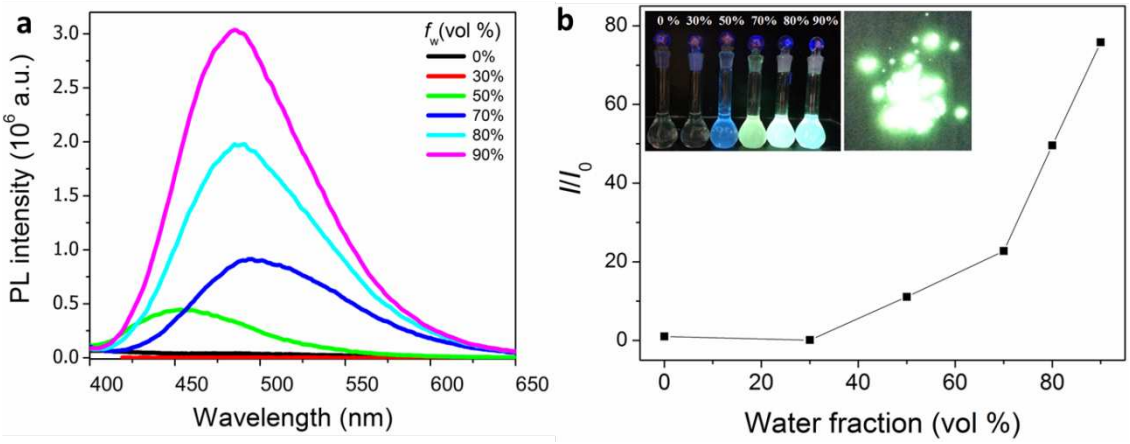

Figure 3. a) Fluorescence spectra of TPE-2PBN in THF/water mixtures with different water fractions (f_w); $\lambda_{excitation}$ = 360 nm. b) Plot of (I/I_0) values versus the compositions of the aqueous mixtures. I_0 = emission intensity in pure THF solution. The inset graph is fluorescence images of TPE-2PBN in THF/water mixtures with different water fractions (f_w) and powder state taken under UV illumination.

Both compounds display very poor emission in common organic solvents, such as CH_2Cl_2 and THF, while strong emissions are observed in their neat film. This result clearly implies TPE-PBN and TPE-2PBN could possess an AIE behaviour. Therefore, the photoluminescent (PL) property of these novel compounds were investigated in THF solution and THF/water mixtures. In order to clearly understand the AIE property, TPE-2PBN is taken as a detailed example to discuss (Figure 3). In pure THF solution, TPE-2PBN could not emit any light under UV illumination with 360 nm excitation wavelength. After addition of water into THF solution, AIE behaviour is clearly observed, further evidenced by the plot of fluorescence intensity (Figure 3b) and the photographs (Figure 3b inset) in THF/water mixture with different water fraction (f_w, 0-90%). As illustrated in Figure 2a, the emission intensity has a negligible change from 0% to 30% water fraction. Subsequently, the PL spectrum reveals significant increased emission intensity at

50% water fraction, accompanied with an abnormal blue shift (ca. 35 nm). From f_w of 70%, the emission intensity increases gradually, and the strongest emission intensity is obtained at f_w of 90%. The PL intensity of TPE-2PBN at 90% water fraction is about 76 folds higher than that in pure THF (I_{90}/I_0, Figure 3b). According to the previous reports, this result implies TPE-2PBN possesses a typical AIE behaviour. Compared to TPE-PBN, compounds TPE-2PBN shows a better AIE performance owing to the more twist structures of TPE-2PBN (Figure S5b). The luminescent lifetimes (τ) are evaluated to be 1.51 ns and 1.44 ns for TPE-PBN and TPE-2PBN, respectively, suggesting that the emission originates from fluorescence (Figure S6, Table 2). All compounds display a strong emission in neat film with the maximum peaks in the range of 477-490 nm (Figure S7). Furthermore, their pristine powders show brighter fluorescence from blue to blue-greenish emission with quantum yield (Φ_F) of 71% and 83% for TPE-PBN and TPE-2PBN, respectively.

3.4 Theory Calculations

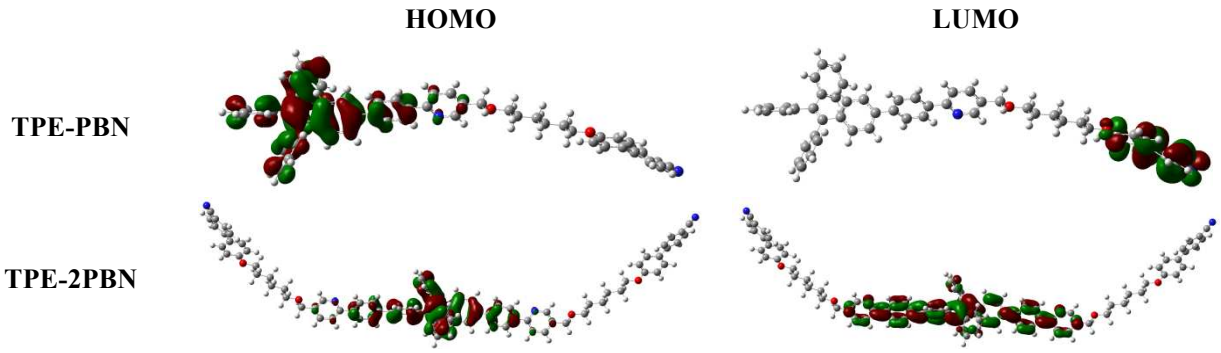

Figure 4. Molecular orbital distributions of compounds TPE-PBN and TPE-2PBN

To further investigate the relationship between molecular structure and electronic delocalised property, density functional theory (DFT) calculation with Gaussian 09 program using B3LYP

functional were carried out. The calculated HOMO and LUMO of all compounds are shown in Figure 4. The optimised geometrical structures reveal that these compounds have a steric structure due to the TPE core. For compound TPE-PBN, the HOMO is mainly localised on TPE core with some contribution from phenylpyridine unit while the LUMO is localised on 4-cyanobiphenyl moiety. The spatially separated HOMO and LUMO distributions imply that a charge-transfer process can occur in TPE-PBN. The HOMO distribution pattern of TPE-2PBN is similar with TPE-PBN, which is mainly localised on TPE core with some contributions from phenylpyridine units. Conversely, its LUMO is distributed on phenylpyridine unit and TPE core rather than 4-cyanobiphenyl moiety. It is noted that the increased arm numbers (phenylpyridine-cyanobiphenyl unit) have an obvious effect on their geometrical structure and electronic distributions. Consequently, these different electronic distribution properties also illustrate the difference in absorption performance.

3.5 Electrochemical property

The electrochemical properties of the compounds were recorded in degassed CH_2Cl_2 solution *via* cyclic voltammetry (CV, ESI†), and the data are summarised in Table 2. TPE-PBN and TPE-2PBN show the irreversible oxidation potentials at 1.30 V and 1.22 V, respectively (*vs* Fc/Fc^+, $E_{Fc/Fc+}$ = 0.44 V), while the irreversible reduction potentials are observed in the range -1.84 V (TPE-PBN) and –1.72 V (TPE-2PBN). According to the formula of $E_{HOMO} = -(E_{ox} + 4.8)$ eV and $E_{LUMO} = -(E_{red} + 4.8)$ eV, the HOMO/LUMO values are calculated to be –6.10/–2.96 eV and –6.02/–2.98 eV for TPE-PBN and TPE-2PBN, respectively. Compared with TPE-PBN, TPE-2PBN shows an increased HOMO level and a decreased LUMO level, leading to a narrower

band energy gap. Obviously, the number of mesogenic unit has a clearly effect on the HOMO and LUMO values, which matches well with the calculated result.

3.6 Hole Mobilities

The hole mobilities of TPE-PBN and TPE-2PBN were measured by SCLC method with a device configuration of ITO/PEDOT:PSS (40 nm)/compound (100 nm)/MoO_3 (10 nm)/Al (100 nm), and the *J-V* (current density-voltage) curves are shown in ESI† . Both compounds presented the hole mobilities of 2.63×10^{-5} and 4.17×10^{-5} $cm^2 V^{-1} s^{-1}$ (ESI†) in the pristine film, respectively. After the active layer annealing at 165ºC, TPE-PBN and TPE-2PBN showed an enhanced hole mobilities in the range of 10^{-4} $cm^2 V^{-1} s^{-1}$ (ESI†), which is about an order of magnitude higher than that of pristine film. This result implies that the self-assembly property of liquid crystal plays an important role on the hole mobilities.

3.7 Electroluminescent property

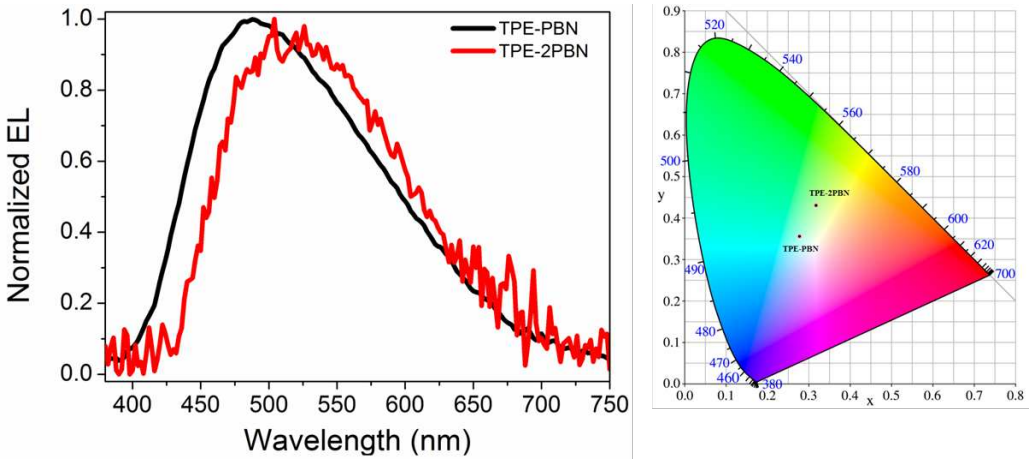

Figure 5. Normalised EL spectra and CIE coordinates of TPE-PBN and TPE-2PBN based non-doped devices

To evaluate the electroluminescent (EL) performance of these AIE molecules, the non-doped OLED devices employing TPE-PBN and TPE-2PBN as the emitter were initially fabricated with the configuration of ITO/PEDOT:PSS (40 nm)/compounds (40 nm)/TmPyPB (50 nm)/Liq (1 nm)/Al (100 nm). In the device structure, TmPyPB is served as an electron-transporting layer (ETL). As shown in Figure 5a, TPE-PBN-based non-doped device presents a blue-greenish EL emission with the peak at 488 nm, while the TPE-2PBN-based device displays a yellowish-green EL emission with the peak at 504 nm. Consequently, the Commission Internationale de l'Éclairage (CIE) color coordinates of (0.28, 0.36) and (0.32, 0.43) are obtained for TPE-PBN and TPB-2PBN based non-doped devices, respectively (Figure 5b). However, the non-doped devices show an undesirable performance, which is summarised in Table S1. The TPE-PBN-based non-doped devices achieved a maximum luminance of 140 cd m^{-2} (117 mA cm^{-2}) and a current efficiency of 1.04 cd A^{-1} (Figure S9 and S10). Compared to the TPE-PBN-based device, TPE-2PBN-based device reveals an inferior performance with a maximum luminance of 15 cd m^{-2} (33 mA cm^{-2}) and a current efficiency of 0.07 cd A^{-1}. This poor device performance could be ascribed to the poor charge carrier transport in the emitter.

Table 3 Performances of doped OLEDs[a] based on TPE-PBN and TPE-2PBN

compound	V^b /V	$\lambda_{EL}{}^c$ /nm	CE^d /cd A^{-1}	PE^e /lm W^{-1}	L^f /cd m^{-2}	EQE^g /%
TPE-PBN	9	469	6.2	2.0	1308	4.1
TPE-2PBN	9	478	2.7	0.6	1612	1.5

a: OLEDs device configurations: ITO/PEDOT:PSS (40 nm)/ mCP:compound (99:1, 20 nm)/TmPyPB (50 nm)/Liq (1 nm)/Al (100 nm); b: turn-on voltage at 1 cd m^{-2}; c: maximum emission peak; d: maximum current efficiency; e: maximum power efficiency; f: maximum luminance; g: external quantum efficiency ;

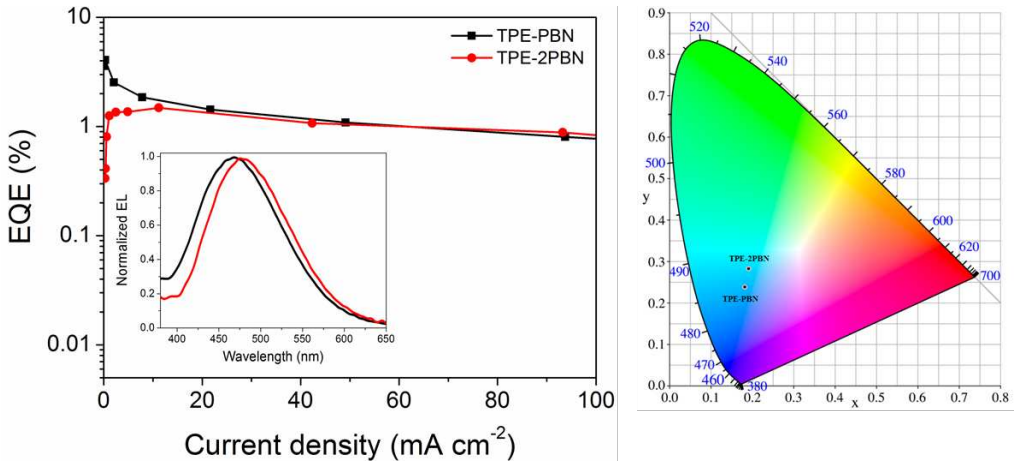

Figure 6. External EL quantum efficiency (η_{ext}) curves, EL spectra (inset) and CIE coordinates of TPE-PBN and TPE-2PBN based doped devices

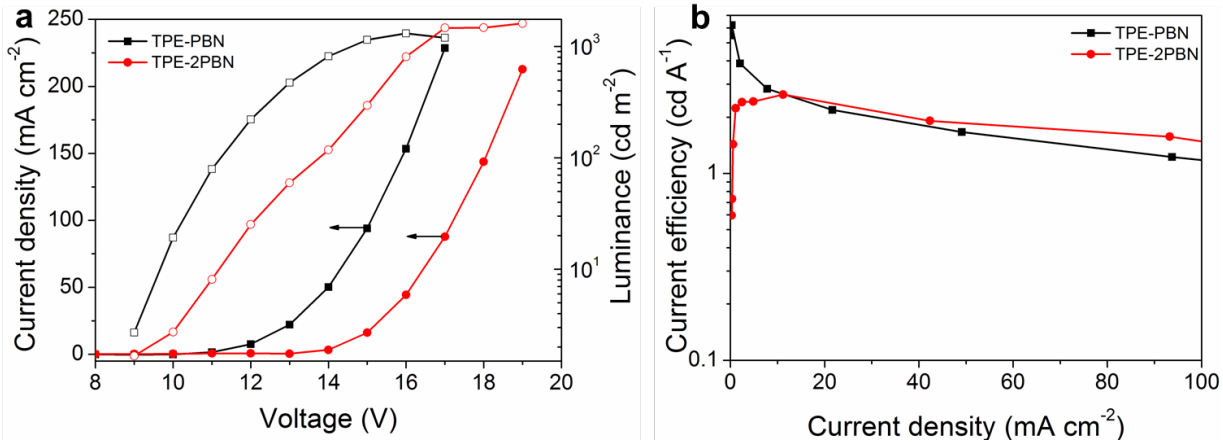

Figure 7. Current density–voltage–luminance (*J*–*V*–*L*) characteristics (a) and current efficiency curves (b) of TPE-PBN and TPE-2PBN based doped devices

In order to improve the device performance, the OLED using mCP as the host matrix and TPE-PBN and TPE-2PBN as dopants with the configuration of ITO/PEDOT:PSS (40 nm)/mCP:compound (99:1, 20 nm)/TmPyPB (50 nm)/Liq (1 nm)/Al (100 nm) are fabricated for comparison. The narrow emitting layer was designed based on the consideration of the inferior charge transporting property of the emitter. In this device structure, mCP is used to the host matrix due to its high triplet energy level (2.9 eV).[40] The bright blue emission with the maximum peak at 469 nm and 478 nm are attained for the TPE-PBN- and TPE-2PBN-based device, respectively, and their CIE coordinated are located on (0.18, 0.24) and (0.19, 0.28) (Figure 6).

The current density-voltage-luminance curves and current efficiency characteristics are presented in Figure 7a, and the EL data are list in Table 3. Both devices possess a relatively high turn-on voltage of 9 V (a luminance of ca. 2 cd m^{-2}), presumably due to the unbalance charge-carrier mobilities in these devices. It is noted that the performances of these host-guest devices are much better than those of the non-doped devices. The TPE-PBN-based device shows a maximum luminance of 1308 cd m^{-2} (16 V, 153 mA cm^{-2}) and a current efficiency (CE) of 6.2 cd A^{-1} (Figure 7b). Furthermore, a promisingly high EQE of 4.1 % was achieved for the TPE-PBN based device, which is close to the theory EQE upper-limit value (ca. 5 %) for the blue fluorescent OLED. The device based on TPE-2PBN also render a decent performance with a highest luminance of 1612 cd m^{-2} (19 V, 213 mA cm^{-2}), a CE of 2.7 cd A^{-1} and an EQE of 1.5 %. It is clearly demonstrated that the number of substituents on TPE core plays a key role in the EL performance.

4 CONCLUSIONS

In summary, two novel AIE-based LLC molecules of TPE-PBN and TPE-2PBN were fortunately synthesised. Although both compounds possess a simple molecular structure without much periphery flexible chains, thermotropic liquid crystalline property were achieved. Higher hole mobilities, in the range of 10^{-4} $cm^2v^{-1}s^{-1}$, were found for the annealed film compared to the pristine film. As expected, TPE-PBN and TPE-2PBN displayed intense blue/blue-greenish light with high emission quantum of 71% and 83% in the solid state. Both of the luminescent liquid crystal molecules can effectively act as the EL emitter in the devices. The doped devices based on TPE-PBN showed a better performance with a current efficiency of 6.2 cd A^{-1} and a high external quantum efficiency of 4.1 %. Obviously, this research demonstrates that by utilising the

combination of AIE luminogens and the mesogenic properties should be an ideal strategy for design the highly efficient luminescent liquid crystal materials.

ASSOCIATED CONTENT

Supporting Information

The Supporting Information is available free of charge on the ACS Publications website.

AUTHOR INFORMATION

Corresponding Author

*E-mail: qiji830404@hotmail.com (Y. Wang)

*E-mail: guohua.xie@whu.edu.cn (G. Xie)

*E-mail: duncan.bruce@york.ac.uk (D. W. Bruce)

*E-mail: zhuwg18@126.com (W. Zhu)

Author Contributions

The manuscript was written through contributions of all authors. All authors have given approval to the final version of the manuscript.

ACKNOWLEDGEMENT

CPC thanks the University of York for financial support. The X-ray diffractometer in York was purchase with funds from EPSRC. We thank the financial support from Natural Science Foundation of Hunan Province (2017JJ2245, 14JJ2081), The Petrochemical Joint Fund Between the National Natural Science Foundation & China Petroleum and Chemical Corporation (U1663229), the Program for Innovative Research Cultivation Team in University of Ministry of Education of China (1337304) and the Talent project of Jiangsu Specially-Appointed Professor.

REFERENCES

1. M. O'Neill and S. M. Kelly, *Adv. Mater.*, 2003, **15**, 1135-1146.
2. Y. Wang, J. Shi, J. Chen, W. Zhu and E. Baranoff, *J. Mater. Chem. C*, 2015, **3**, 7993-8005.
3. S. Setia, S. Sidiq, J. De, I. Pani and S. K. Pal, *Liquid Crystals*, 2016, **43**, 2009-2050.
4. Y. F. Wang, J. Fan, J. w. Shi, H. R. Qi, E. Baranoff, G. H. Xie, Q. G. Li, H. Tan, Y. Liu and W. G. Zhu, *Dyes and Pigments*, 2016, **133**, 238-247.
5. R. J. Bushby, S. M. Kelly and M. O'Neill, Liquid crystalline semiconductors: materials, properties and applications, *Volume 169 of the series Springer Series in Materials Science*, ISSN: 0933-033X, Springer, 2013, **Chapter 7,** 197-218.
6. S. Liu, M. Lin, L. Chen, Y. Hong, C. Tsai, C. Wu, A. Poloek, Y. Chi, C. Chen, S. Chen and H. Hsu, *Org. Electron*, 2011, **12**, 15-21.
7. A. Contoret, S. Farrar, P. Jackson, S. Khan, L. May, M. O'Neill, J. Nicholls, S. Kelly and G. Richards, *Adv. Mater.*, 2000, **12**, 971-974.
8. M. Grell, and D. D. C. Bradley, *Adv. Mater.*, 1999, **11**, 895-905.
9. H. Singh, A. Balamurugan and M. Jayakannan, *Appl. Mater.*, 2013, **5**, 5578-5591.
10. X. M. He, J. B. Lin, W. H. Kan, P. C. Dong, S. Trudel and T. Baumgartner, *Adv. Funct. Mater.*, 2014, **24**, 897-906.
11. H. Tokuhisa, M. Era and T. Tsutsui, *Appl. Phys. Lett.*, 1998*,* **72**, 2639-2641.
12. S.Thiery, B. Heinrich, B. Donnio, C. Poriel and F. Camerel, *J. Mater. Chem. C*, 2014, **2**, 4265-4275.
13. B. Zhang, C. H. Hsu, Z. Q. Yu, S. Yang and E. Q. Chen, *Chem. Commun.*, 2013, **49**, 8872-8874.
14. R. Gimenez, M. Pinol and J. L. Serrano, *Chem. Mater.*, 2004, **16**, 1377-1383.
15. S. Moyano, J. Barbera, B. E. Diosdado, J. L. Serrano, A. Elduque and R. Gimenez, *J. Mater. Chem. C*, 2013, **1**, 3119-3128.
16. E. Beltran, J. L. Serrano, T. Sierra and R. Gimenez, *J. Mater. Chem.*, 2012, **22**, 7797-7805.
17. A. Liedtke, S. M. Kelly, S. P. Kitney, B. V. Averbeke, P. Boudard, D. Beljonne and J. Cornil, *J. Phys. Chem. B*, 2010, **114**, 11975-11982.
18. R. Cristiano, J. Eccher, I. H. Bechtold, C. N. Tironi, A. A. Vieira, F. Molin, and H. Gallardo, *Langmuir*, 2012, **28**, 11590-11598.
19. Y. Sagara and T. Kato, *Angew. Chem. Int. Ed*., 2008, **47**, 5175-5178.
20. S. Yamane, Y. Saqara, T. Mutai, K. Araki and T. Kato, *J. Mater. Chem. C*, 2013**, 1**, 2648-2656.
21. S. Yamane, Y. Saqara and T. Kato, *Chem. Commun.*, 2013, **49**, 3839-3841.

22. M. Mitani, S. Ogata, S. Yamane, M. Yoshio, M. Haseqawa and T. Kato, *J. Mater. Chem. C*, 2016, **4**, 2754-2760.
23. C. Damm, G. Israel, T. Heqmann,and C. Tschierske, *J. Mater. Chem.*, 2006, **16**, 1808-1816.
24. A. M. *T*alarico, M. Ghedini, C. O. Rossi and E. I. Szerb, *Soft Matter.*, 2012, **8**, 11661–11669.
25. J. W. Shi, Y. F. Wang, M. J. Xiao, P. Zhong, H. Tan, Y. Liu, M. X. Zhu and W. G. Zhu, *Tetrahedron*, 2015, **71**, 463-469.
26. Y. F. Wang, Q. Chen, Y. H. Li, H. Tan, Y. Liu, J. T. Yu, M. X. Zhu, H. B. Wu, W. G. Zhu and Y. Cao, *J. Phys. Chem. C*, 2012, **116**, 5908-5914.
27. Y. F. Wang, Y. Liu, J. Luo, H. R. Qi, X. S. Li, M. J. Ni, M. Liu, M. X. Zhu, W. G. Zhu and Y. Cao, *Dalton Trans.*, 2011, **40**, 5046-5051.
28. A. Santoro, A. C. Whitwood, J. A. G. Williams, V. N. Kozhevnikov and D. W. Bruce, *Chem. Mater.*, 2009, **21**, 3871-3882.
29. V. Kozhevnikov, B. Donnio and D. W. Bruce, *Angew. Chem. Int. Ed.*, 2008, **47,** 6286-6289.
30. V. W.-W. Yam, K. H.-Y. Chan, K. M.-C. Wong and B. W.-K. Chu, *Angew. Chem. Int. Ed.*, 2006**, 45**, 6169-6173.
31. J. D. Luo, Z. L. Xie, J. W. Y. Lam, L. Cheng, H. Y. Chen, C. F. Qiu, H. S. Kwok, X. W. Zhan, Y. Q. Liu, D. B. Zhu and B. Z. Tang, *Chem. Commun.*, 2001, **18**, 1740−1741.
32. J. Mei, N. L. C. Leung, R. T. K. Kwok, J. W. Y. Lam and B. Z. Tang, *Chem. Rev.*, 2015, **115**, 11718-11940.
33. W. Z. Yuan, Z. Q. Yu, P. Lu, C. M. Deng, J. W. Y. Lam, Z. M. Wang, E. Q. Chen, Y. Q. Ma and B. Z. Tang, *J. Mater. Chem.*, 2012, **22**, 3323-3326.
34. C. Li, J. Wei, J. Han, Z. Li, X. Song, Z. Zhang, J. Zhang and Y. Wang. *J. Mater. Chem. C*, 2016, **4**, 10120-10129.
35. W. Qin, Z. Yang, Y. Jiang, J. Lam, G. Liang, H. Kwok and B. Tang, *Chem. Mater.*, 2015, **27**, 3892-3901.
36. K. Kuribayashi, T. Kubota, N. Tanaka, T. Fukuda, T. Tsuji and R. Goto, Japan, 2011049126[P]. 2011-04-28.
37. J. W. Chen, C. C. W. Law, J. W. Y. Lam, Y. P. Dong, S. M. F. Lo, I. D. Williams, D. B. Zhu and B. Z. Tang, *Chem. Mater.*, 2003, **15**, 1535-1546.
38. N. Godbert, A. Crispini, M. Ghedini, M. Carini, F. Chiaravalloti and A. Ferrise, *J. Appl. Cryst*., 2014, **47**, 669-679.
39. D. Y. Zhao, J. Cheng, K. S. Wong, V. G. Chigrinov, H. S. Kwok and L. Guo, *Adv. Optical Mater.*, 2015, **3,** 199-202.
40. J. S. Swensen, E. Polikarpov, A. V. Ruden, L. Wang, L. S. Sapochak and A. B. Padmaperuma, *Adv. Funct.*

Mater., 2011, **21**, 3250-3258.

Graphic Abstract